Experimental and numerical investigation of weak blast wave interaction with a three levels building

Jacques Massoni, Laurent Biamino, Georges Jourdan, Ozer Igra, Lazhar Houas

Experimental and numerical investigation of weak blast wave interaction with a three levels building

Jacques Massoni[1], Laurent Biamino[1], Georges Jourdan[1], Ozer Igra[2] and Lazhar Houas[1]
[1]Aix Marseille Univ, CNRS, IUSTI, Marseille, France
[2]Ben Gurion University, Beer Sheva 84105, Israel; Peter the Great St. Petersburg Polytechnic University, Saint Petersburg 195251, Russia

Key words: Blast waves; blast reflections; blast enhancement; human damages.

Abstract

The present work shows that weak blast waves that are considered as being harmless can turn to become fatal upon their reflections from walls and corners inside a penetrated building. In the experimental part, weak blast waves were generated by using an open-end shock tube. A three level building model was placed in vicinity to the open-end of the used shock tube.

The evolved wave pattern inside the building rooms was recorded by a sequence of schlieren photographs; also pressure histories were recorded on the rooms' walls. In addition, numerical simulations of the evolved flow field inside the building was conducted. The good agreement obtained between numerical and experimental results allows running the used code for identifying safety and dangerous places inside the building rooms penetrated by the weak blast wave.

I Introduction

While it is well known that strong blast waves are lethal for a living creature, it is commonly accepted that weak blast waves are harmless. Although this might be the case when there is a direct impingement of the on-coming weak blast wave on a considered body, a completely different scenario takes place when the weak and quite-safe blast wave hits a body after multiple reflections from existing walls and corners. Such a case can be found when a weak or medium strength blast wave, resulting from a sudden explosion, as the explosion of a gas pipeline in a street for example, hits a residential complex. Furthermore, explosion injuries can be caused by direct hit of a blast wave, flying debris resulting from the explosion, as well as by objects being dragged or pushed by the blast wave [1]. The present investigation focuses on injuries caused by direct hit of the blast wave. Information given in Table 1 (see [1], [2], [3] and [4]) reveals human response to overpressure; this information is used in defining a place as being safe or not-safe.

In the conducted experiments a very simple model of a three levels building is subjected to an initial harmless or quasi-harmless blast wave. The aim of the present study is to find where the most dangerous places inside the building are, places without having death risk, and where are the safest places for people to be. We try to answer the question: does an initially harmless blast wave become dangerous after multiple reflections or not?

A shock tube is used for generating the required quasi-safe blast waves. Initially a weak or medium strength, planar shock wave propagates inside the shock tube. Upon reaching the tube exit-open-end, it immerges into the open atmosphere as a blast wave. The investigated building model is placed in proximity to the shock tube exit. Several positioning have been tested, i.e., close or far from the shock tube exit, always aligned with the shock tube. Finally, an optimized positioning has been found (see Fig. 1). Schematic descriptions and dimensions of the used building model are presented in Fig. 2.

In addition to the experimental investigation, numerical simulation of the generated flow field, caused by the blast wave interaction with the building model, is conducted in order to observe the overpressure reached in places where pressure-sensors installment are not possible.

In urban life, blast waves can be generated from a sudden explosion of gas lines placed underground, from a truck carrying an explosive substance in a residential neighborhood, or from a terrorist attack in the public domain.
Considering weak quasi-safe blast waves, all these examples have one thing in common, i.e., the fact that generally people are not informed of potential risks to their ears or lungs, not to mention life, if they stand in proximity to a wall or a corner close to where a blast wave propagates. Subsequently, it will be shown where are the dangerous places inside a residential building in a case that the building is impacted by an initially quasi-safe blast wave.

From a fluid mechanics point of view, the present work deals with the problem of multiple shock or blast wave reflections. This topic was treated in many publications; e.g., in Ben-Dor [5], Igra et al. [6] and more recently, in Volume 2 of the Handbook of Shock Waves by Ben-Dor, Igra and Elperin [7].

Table 1: Direct effects of a blast wave generated overpressure on humans for a blast wave surface covering a human and without encountering any obstacle (from [1], [2], [3] and [4]).

Overpressure (KPa)	Direct effects on human
<3	No data
6	People projected on the ground
8	Danger for eardrums
12 (+/- 5)	Destruction of 1% of eardrums
40	Destruction of 99% of eardrums
60	Danger for lungs
100 – 500 (+/- 20)	Destruction of 50% of lungs
100	1% death
350	99% death

Direct effects means without considering secondary (indirect) effects such as flying glass or brick debris which start from about 3 to 5 KPa. Note that values given by medical references (from locations where humans have been affected by explosions) are slightly higher than those deduced from shock and blast wave experiments.

II Experimental set-up

The present experiments were conducted using an open end shock tube and thereby generating weak and moderate blast waves. The generated blast waves were sufficiently weak to ensure that they pose no life endangerment to people, but are intense enough to cause irreversible damage, e.g., to eardrums.
The building model was constructed from Plexiglas in order to allow high speed shadowgraph and schlieren visualizations. The facility used is shown in Fig. 2. The used optical facility is composed of two mirrors, one spherical, used for converting a parallel light beam into a converging one, and the other, planar, for simply reflecting parallel beam without any change. Both mirrors belong to the shadowgraph and the schlieren device.

Experiments were conducted using the T80 horizontal shock tube. It has a total length of 3.75 meters, a high pressure chamber 0.75 meters long followed by a low pressure section of 3 meters length, and an 8 cm by 8 cm square cross section. It is equipped with the SA1 PHOTRON high speed shadowgraph or schlieren visualization device, PCB pressure transducers and Tektronix digital oscilloscopes. It was used keeping its exit open. All present

visualizations were taken with a frequency of 30,000 frames per second. Detailed description of this shock tube can be found in [8].

To simplify the experimental set-up, both the Plexiglas building model and the shock tube were positioned horizontally. Therefore, if the reader wants to observe the schlieren images as if the blast wave comes from the building bottom toward its top, he should rotate the images by 90^0, as we have made for results presented subsequently. The building was modeled very simply. It consists of three cubic boxes simulating three levels of one-room-apartments. All apartments had no frontal wall and no glass windows; this was done for avoiding broken glass or flying brick segments. The first floor consists of an empty box. The second was identical box but it had a dividing wall and an open door in its center. The third level had the same dividing wall to which an opened window was added on the box back wall. As mentioned, detailed descriptions of the Plexiglas building and its positioning relative to the shock tube exit are given in Fig. 2. Finally, for validation of the used simulations three pressure gauges were installed at the center of each room back-wall. Thus, experimental and numerical results could be compared and thereby validating the used simulation.

Due to the small size of the investigated building model and in order not to disturb the flow and wave reflections inside the building model, pressure gauges were not installed during the first runs. Once installed, visualizations were no more possible. Nevertheless, pressures prevailing at multiple locations inside the building model were deduced from numerical simulation of the experiments after ensuring a very good agreement between measurements and numerical simulations.

One series of experiments was undertaken in order to generate a very weak planar shock wave inside the shock tube. Upon exiting the shock tube it quickly becomes a weak blast wave. In the first series of experiments the Mach number of the incident shock wave M_{is} was $1.11 \leq M_{is} \leq 1.17$. It is sufficiently weak to ensure that the generated blast wave creates an overpressure ΔP about 4 to 5 KPa when entering the first floor of the building (see Fig. 3a). Such a blast wave is of no danger to people.

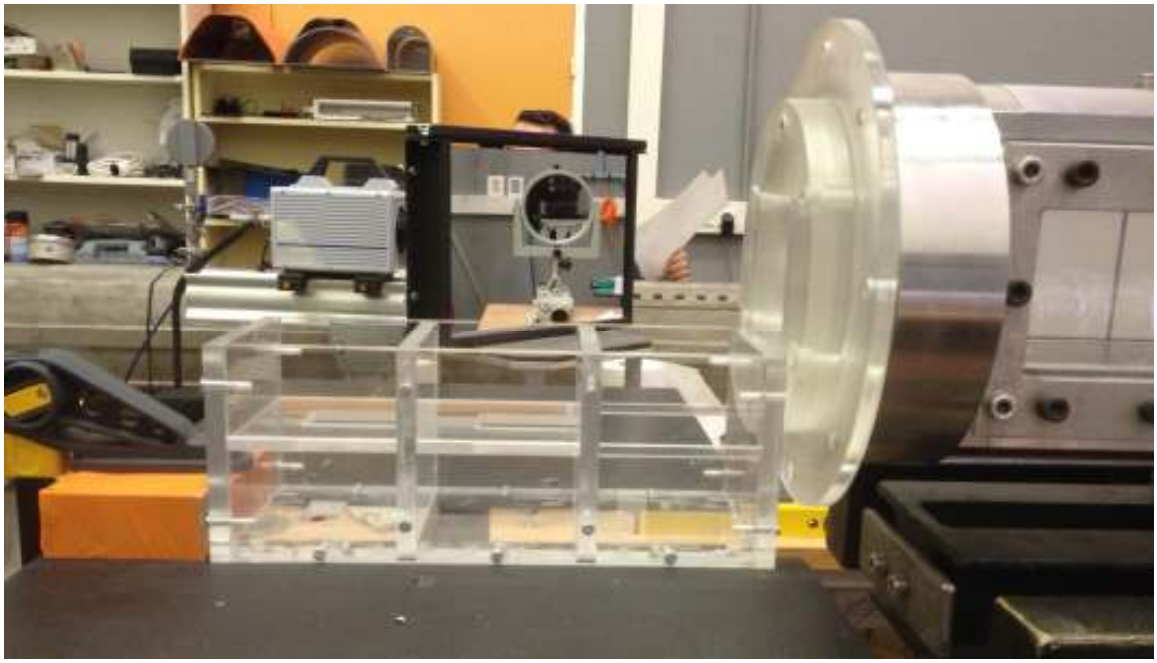

Figure 1: View of the Plexiglas building model located close to the shock tube exit. For simplicity both the Plexiglas building and the shock tube are positioned horizontally (gravity effects are negligible in such case).

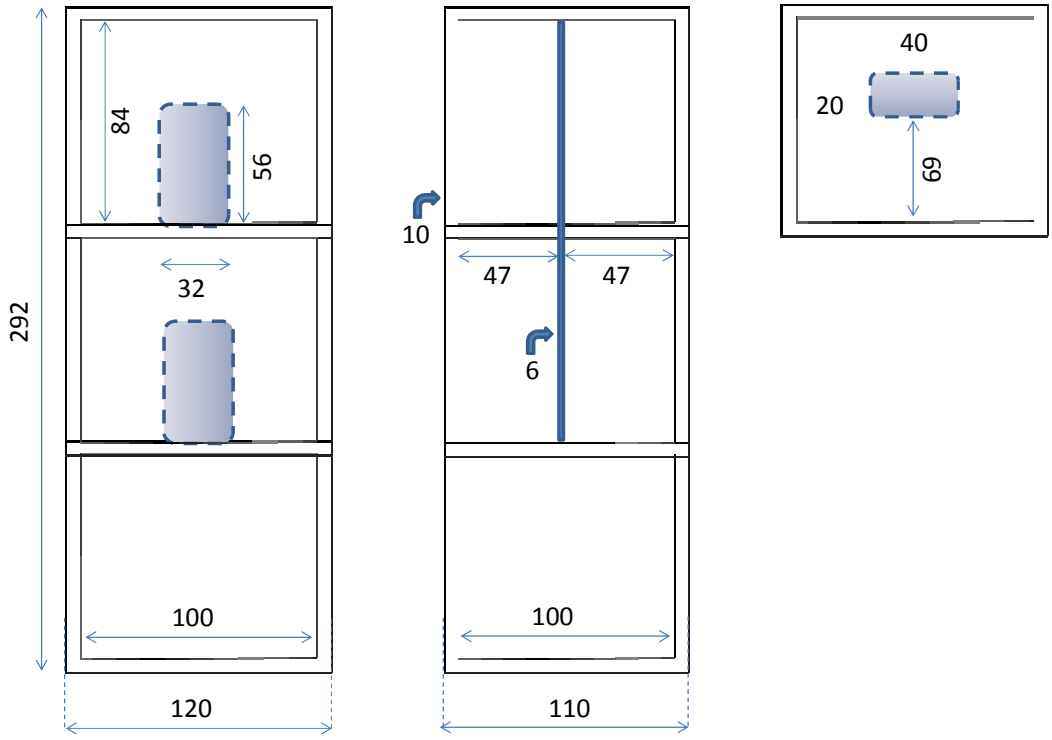

(a)

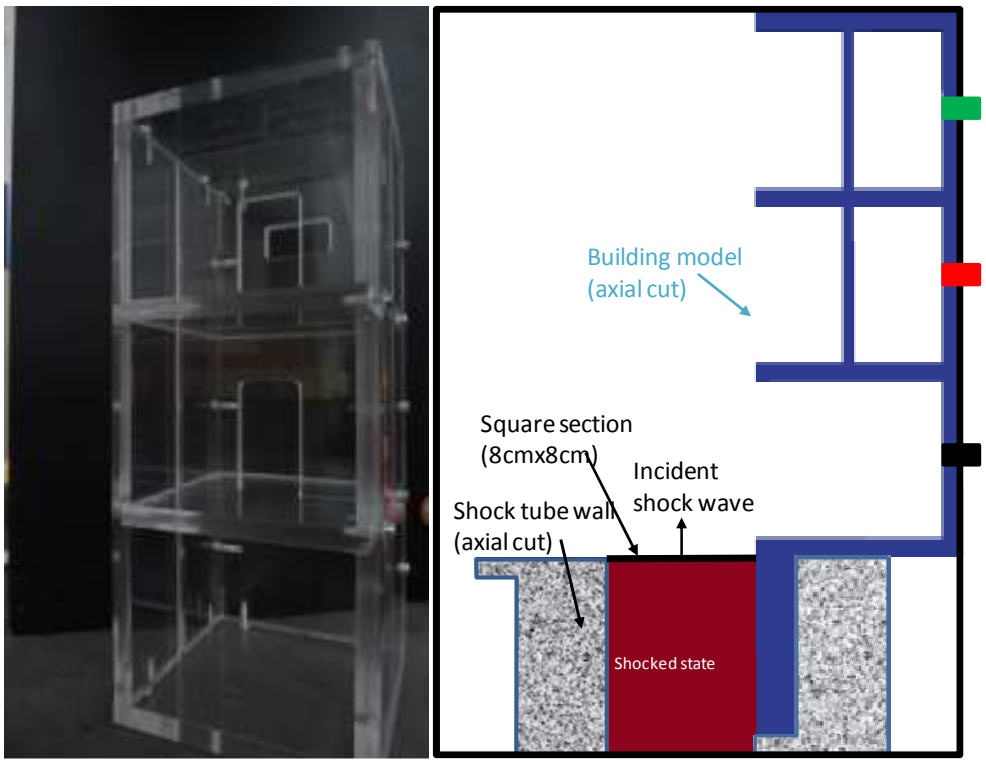

(b) (c)

Figure 2: Description and dimensions of the tested building model, (a) schematic drawing of the model (units are in mm), (b) a photo of the Plexiglas model, and (c) its location relative to the shock tube exit. Black, red and green represent the pressure gauge locations of ground, second and third levels, respectively. Dark-red color represents the shocked air flow inside the shock tube before the shock wave exit.

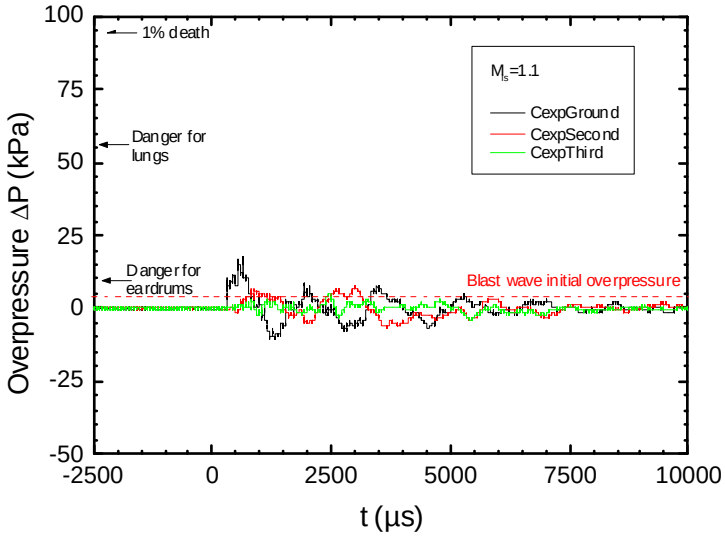

(a)

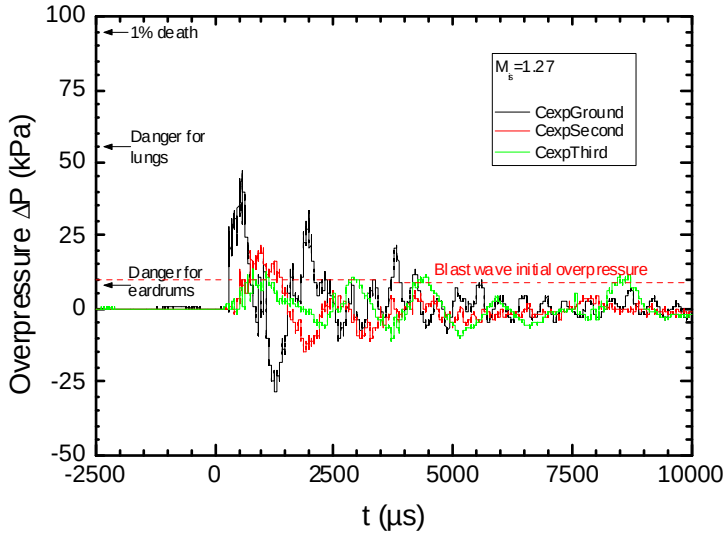

(b)

Fig. 3: Overpressure signals recorded at the center of the ground floor wall, the second floor wall and the third floor wall.

It is clear from Fig. 3 that upon entering the first floor the blast wave experiences a four time overpressure increase relative to its initial overpressure, which was about 4 KPa in the case shown in Fig. 3a (M_{is}=1.11); the same is evident in Fig. 3b where the initial overpressure of 10 KPa is raised to about 40 KPa in the case were M_{is}=1.27. M_{is} is the Mach number of the incident straight shock wave inside the shock tube. It should be noted that the overpressure reached close to the room corners is even higher than that prevailing at the wall center as shown subsequently where results from numerical simulations are discussed.

III Numerical simulation

All computations are performed for air. Due to the low Mach number of the incident shock wave it can be treated as a perfect gas. The conservation equations for ideal compressible fluids (the Euler equations), indicating conservation of mass, momentum and energy are:

$$\frac{\partial \rho}{\partial t} + \nabla.(\rho \boldsymbol{u}) = 0 \qquad (1)$$

$$\frac{\partial \rho \boldsymbol{u}}{\partial t} + \nabla.\boldsymbol{u}\otimes\boldsymbol{u} + P\bar{\bar{I}}_d = 0 \qquad (2)$$

$$\frac{\partial \rho E}{\partial t} + \nabla.(\rho \boldsymbol{u}E + P\boldsymbol{u}) = 0 \qquad (3)$$

where P is pressure (Pa), ρ is density (kg/m^3), $\boldsymbol{u}$ is the velocity vector (m/s), I_d is the identity tensor and

$$E = e + \frac{1}{2}\boldsymbol{u}\cdot\boldsymbol{u} \qquad (4)$$

is the total energy. "*e*" stands for the internal energy of the fluid (J/kg). For closing the above set of equations the following ideal gas equation is used:

$$P = \rho r T \qquad (5)$$

$P = \rho r T$

where T is temperature (K). The specific mass gas constant "*r*" is defined by:

$r = \frac{R}{W}$

$$r = \frac{R}{W} \qquad (6)$$

where R is the universal gas constant (J/mol/K) and W is the molar mass of air: W=28.97 10^{-3} kg/mol.

Denoting by

$$U = \begin{bmatrix} \rho \\ \rho \boldsymbol{u} \\ \rho E \end{bmatrix} \qquad (7)$$

the conservative vector and

$$F(U) = \begin{bmatrix} \rho \boldsymbol{u} \\ \rho \boldsymbol{u}\otimes\boldsymbol{u} + P\bar{\bar{I}}_d \\ \rho \boldsymbol{u}E + P\boldsymbol{u} \end{bmatrix} \qquad (8)$$

the corresponding flux, the previous system may be written alternatively in the following conservative form:

$\frac{\partial U}{\partial t} + \nabla.(F(U)) = 0$

$$\frac{\partial U}{\partial t} + \nabla.(F(U)) \qquad (9)$$

This system is solved using a fixed 3D Cartesian grid and employing a Godunov type finite volume scheme (see for example in [9]). This scheme provides second order accuracy while using the MUSCL-Hancock approach [9, 10, 12]. In the following, only a brief description of the main steps in the procedure used is outlined.

Let Δx, Δy and Δz be the discretization steps in the x, y and z directions, respectively and Δt the time step. The volume of a cell mesh is V= $\Delta x.\Delta y.\Delta z$. The mean value of the solution in the cell (ijk) at time t^n is denoted by:

$$U_{ijk}^n = \frac{1}{V}\int_V U(x,y,z,t^n)\,dV \qquad (10)$$

$U_{ijk}^{n} = \frac{1}{V}\int_V U(x,y,z,t^n)dV$

Obtaining the U_{ijk}^{n+1} value at time $t^{n+1} = t^n + \Delta t$ results from the succession of steps, in each direction of space:

- Compute the conservative variables slopes on each cell and slope limitation process (see in [9, 11] for example)
- Prediction of conservative variables at half time step $t^{n+1/2}$ at the level of cells interfaces
- Riemann problem solution at each cell interface

Finally, the conservation step is applied on each cell:

$$U_{ijk}^{n+1} = U_{ijk}^{n} + \frac{\Delta t}{V}\sum_k S_k F_k^{*,n+1/2} n_k \qquad (11)$$

$$U_{ijk}^{n+1} = U_{ijk}^{n} + \frac{\Delta t}{V}\sum_k S_k F_k^{*,n+1/2} \boldsymbol{n}_k$$

On a 3D Cartesian mesh (hexahedral), *k* varies from 1 to 6.
Notations are:
$F_k^{*,n+1/2}$ is the flux solution of the Riemann problem solved from the predicted variables,
S_k is the surface of the interface between cells on face k, and
n_k is the external normal of this last surface.

Concerning the Riemann problem solution, one may use either an exact solution method - that exists for the perfect gas equation of state – or an approximate Riemann solver. An HLLC-type approximate solver as described first in [14] has been used in the present work, it is faster than the exact one [9] and sufficiently precise. Finally, note that the time step Δt must verify the CFL condition throughout the mesh domain:

$$\Delta t < min\left\{\frac{\Delta x}{S_x^n}, \frac{\Delta y}{S_y^n}, \frac{\Delta z}{S_z^n}\right\} \qquad (12)$$

where S^n is the fastest wave speed at time "n" in each direction. For better performance, the numerical code has been parallelized by using MPI libraries. The number of used cells was 1875000; the cell size was 2 mm in each direction. The choice of the size of the mesh was dictated by the desire of a good representation of the results, as well as by that of reducing the calculation times. The main element of this choice is Fig. 6 where we can see that, with exactly the same mesh, we obtain an almost perfect agreement between computations and experiments and that, for two different incident Mach numbers. The waves dynamics (incident, reflected, after crossing...) are in very good correspondence. Even small vorticity zones near the exit of the shock tube are well represented. This choice is then reinforced by the comparisons of the results on pressure gauges (Fig. 7) and validate the results presented on Fig. 8 and Fig. 9. Going back to one the final perspective of this work (real scale situations), it is very important to verify that the using of very fine mesh is not necessary to obtain good results: the calculation time would become unacceptable.

A special treatment was applied to the mesh in order to account for the presence of the shock tube and the building, treated their walls as perfect reflective walls. Under the hypothesis of symmetry, only one half of the real experimental set is computed, cut in the plane as shown in figure 4.

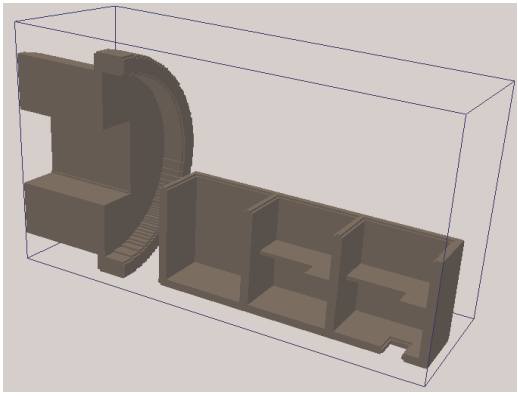

Figure 4: Representation of principle of the computational domain, highlighting the shock tube and the building model with axial symmetry.

IV Results and discussion

A sequence of schlieren photos showing a weak blast wave interaction with the building model is shown in Figure 5. In this case the incident shock wave Mach number inside the shock tube was M_{is}=1.17. At t=33 μs the blast wave is starting its interaction with the building model. With increasing time the blast wave penetrate into the building and at t=200 μs it is clearly seen inside the first floor, approaching the room ceiling. From the darkness intensity of the blast wave it is apparent that the part which penetrated into the building first floor is weaker than the part propagating in the open atmosphere.

At t=300 μs the following waves are visible: the progressing main blast wave starts penetrating into the building second floor while the part penetrated into the first floor is seen now reflected from the first floor ceiling. As noticed earlier, the strongest part of the blast wave, at t=300 μs, is the one propagating through the open atmosphere. However, the darkness intensity of the regular reflection of the blast wave from the ceiling of the first floor room increases, indicating a strengthening blast wave at this location; see in Fig. 5 at t=300 and 333 μs. Further confirmation of the local pressure increase, prevailing around the blast reflection in the considered time is evident in Figs. 8 and 9 to be discussed subsequently. It is apparent from Fig. 5 that the cause for this overpressure increase near the corner is the blast reflection from the room ceiling and wall. It is apparent from Fig. 8 (showing the case of the weakest blast wave, where the generating shock wave Mach number was only 1.11) that at the upper corner of the first floor room the overpressure approaches 35 KPa. This is the strongest overpressure inside the building model witnessed during the considered experiment. As is evident from Table 1 this overpressure is not fatal, however it can cause serious damage to human eardrums. A slightly stronger blast wave could result in irreversible damage, i.e., fatal results. With increasing time, 800 μs ≤ t ≤ 1033 μs multiple wave reflection between the room walls, floor and ceiling takes place as is evident in Fig. 5.

As mentioned, one of the aims of the present work is to explore the overpressure reached in the worst places of the building which were supposed to be the corners. As it is not possible to locate pressure gauges there, the only possibility is to obtain these values from our numerical simulation. But, for that, we need to accurately validate our code. Consequently,

three pressure gauges were installed at the center of each rear wall of the first, second and third floors.

In Figs. 6 and 7, comparison is made between numerically evaluated and experimentally recorded schlieren visualizations; as well as a comparison between recorded overpressure histories (for the cases where the incident shock wave Mach numbers inside the shock tube were M_{is}=1.11 and M_{is}=1.27) and its simulations, respectively. Very good agreement is evident between recorded and simulated schlierens (see Figs. 6a, 6b, 6c and 6d). For clearly showing this agreement lines were added for easily identifying the border/location of the various waves in the two schlieren images. Also, a very good agreement is evident between recorded and simulated overpressures on the first and second floor walls (see Fig. 7). Recorded and computed pressure histories on walls at the third floor are not shown in Fig. 7 since their amplitudes are so low that they are not significant. The oscillations observed in recorded pressures before arrival of the blast wave are due to the fact that the sound velocity in Plexiglas (2500 to 3000 m/s) is about 8 to 10 times higher than that in air (about 340 m/s). Consequently, reflected and refracted blast waves reached and disrupt the pressure gauges by vibratory oscillations before the effective measurement is recorded.

Based on results shown in Figs. 6 and 7, it is safe to conclude that the used numerical scheme is reliable and can safely be used for simulating weak and medium strength blast wave interaction with building.

In Figs. 8 and 9 pressure evolution, resulting from the interaction of a weak (4 KPa over-pressure) and a medium strength (10 KPa over-pressure) blast wave with the three levels building model are shown. As mentioned, it is apparent from Fig. 8 that for the weak blast wave, the acting over-pressure on the ceiling of the first floor, and especially in the corners, is approaching 35 KPa. Such over-pressure is destructive to eardrums (see Table 1) and about 9 times higher than the initial overpressure in the oncoming blast wave. In the case of the medium strength blast wave entering the building model, shown in Fig. 9, the obtained results are more dangerous. The over-pressure in the present case reaches about 70 KPa at the corners of the first floor, which is very dangerous for eardrums, lungs, and could be deadly for frail and old people. As the impinging blast wave propagates into the second and the third floors, no real increase in the post-blast over-pressure is observed due the quick attenuation of the propagating blast wave.

Finally, due to the strong attenuation of the propagating blast wave, when it reach the building third level no comments can be deduced from the present work regarding best location for window in the rear wall of that floor.

V Conclusion

An experimental and numerical investigation of weak and of medium-strength blast wave's interaction with a three levels building has been undertaken using both, a conventional shock tube and numerical simulations. It is clear from the present results that blast wave damages are higher for people standing near a wall, or even higher when near corners. Furthermore, at a late time, the overpressure behind reflected blast wave from a room corner is significantly higher than that experienced in the open atmosphere. This pressure increase is due to blast reflections from the corner between

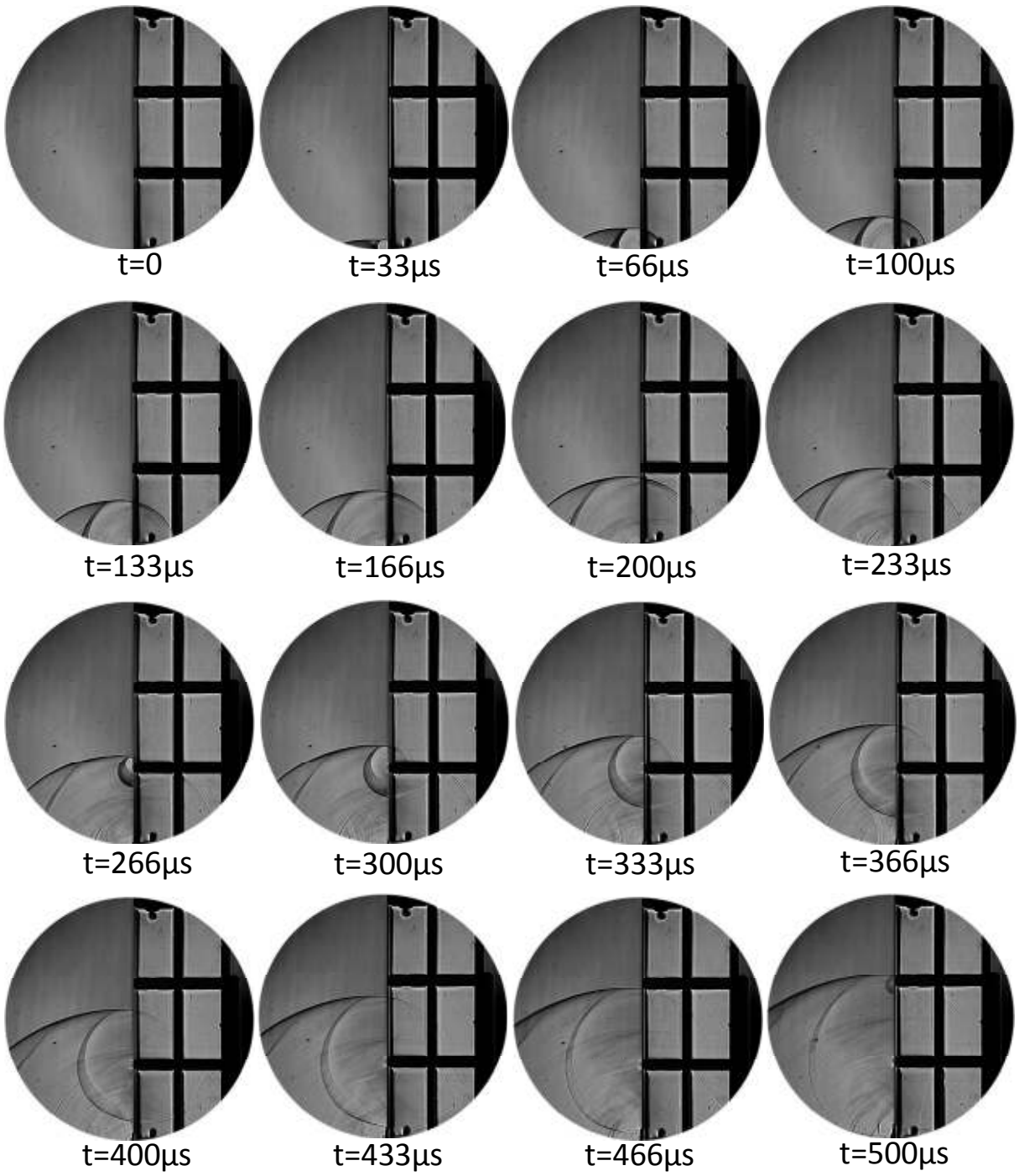

Figure 5: Sequences of schlieren photos (30,000 f/s) showing the evolution and multiple reflections of the blast wave inside the Plexiglas building. The incident shock wave Mach number inside the shock tube was 1.17 (T80#971).

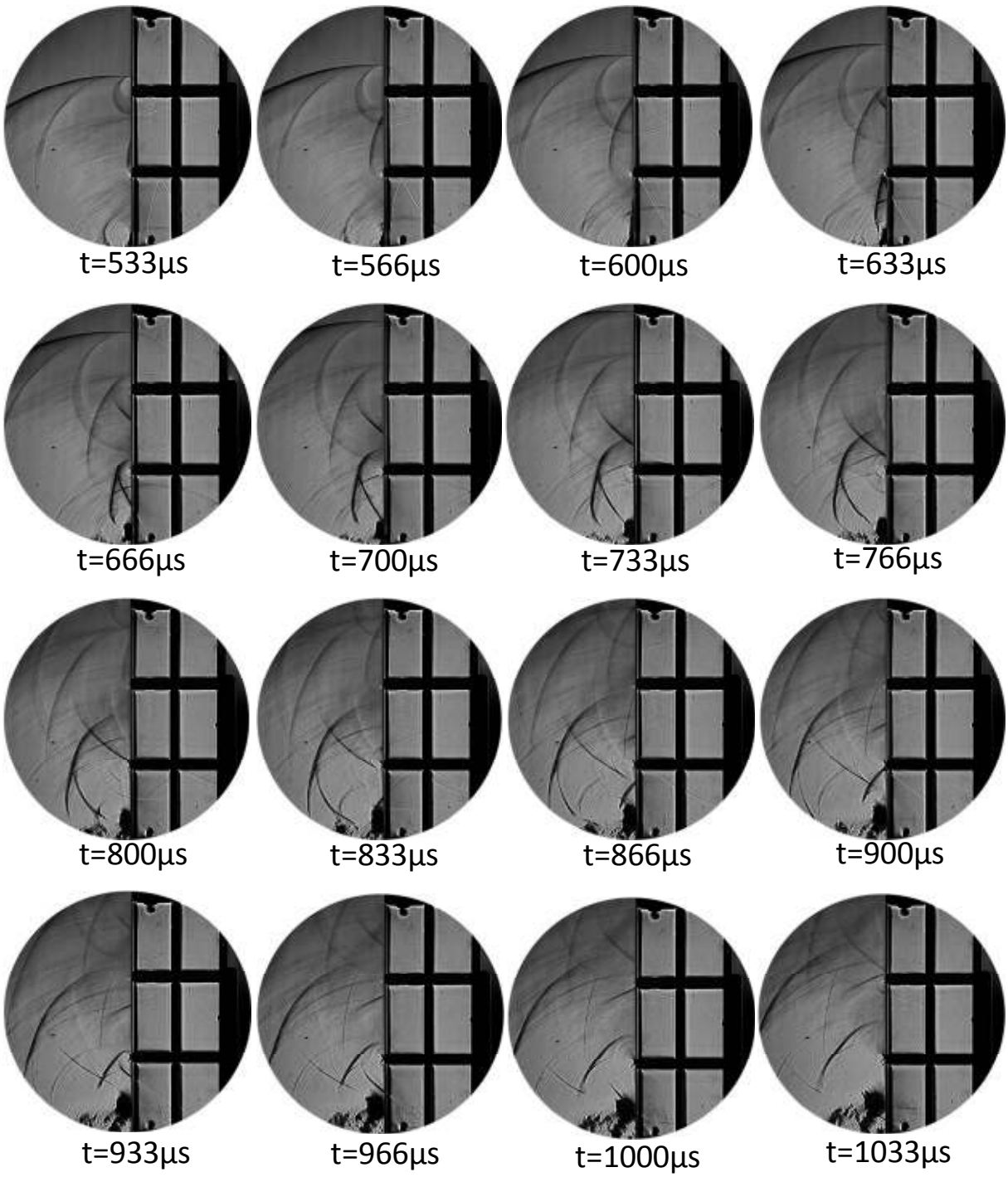

Figure 5 (continue): Sequences of schlieren (30,000 f/s) photos showing the evolution and multiple reflections of the blast wave inside the Plexiglas building. The incident shock wave Mach number inside the shock tube was 1.17 (T80#971).

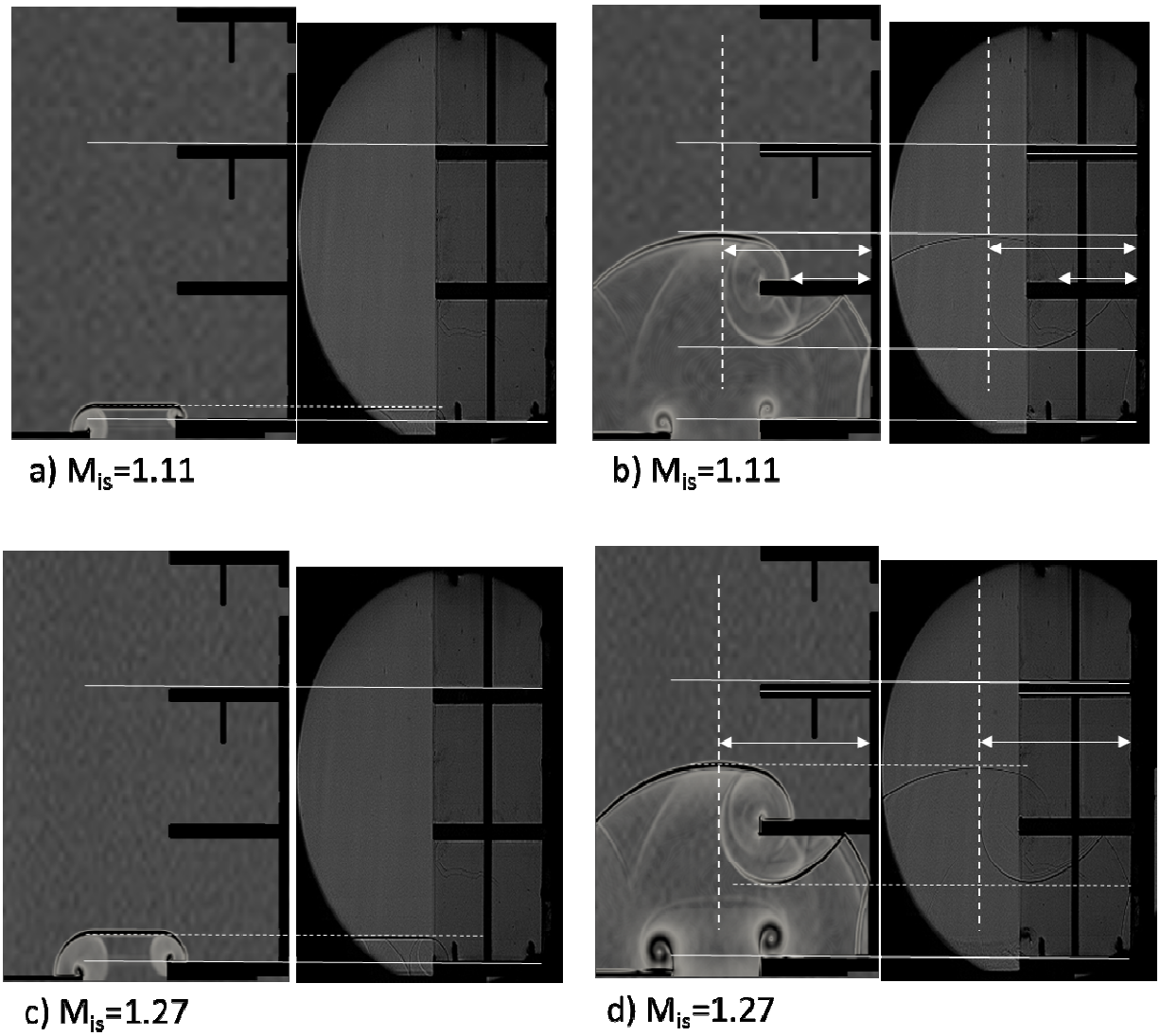

Figure 6: Comparison between schlieren representations obtained from computations (left) and experiments (right). In cases (a) and (b) the incident shock wave Mach number, inside the shock tube, was M_{is}=1.11 (T80#974) and in (c) and (d) it was M_{is}=1.27 (T80#975). Left and right scales are exactly the same, showing a perfect agreement in space and time for waves dynamics. Except from initial -physical- conditions, neither parameter have been change in computations.

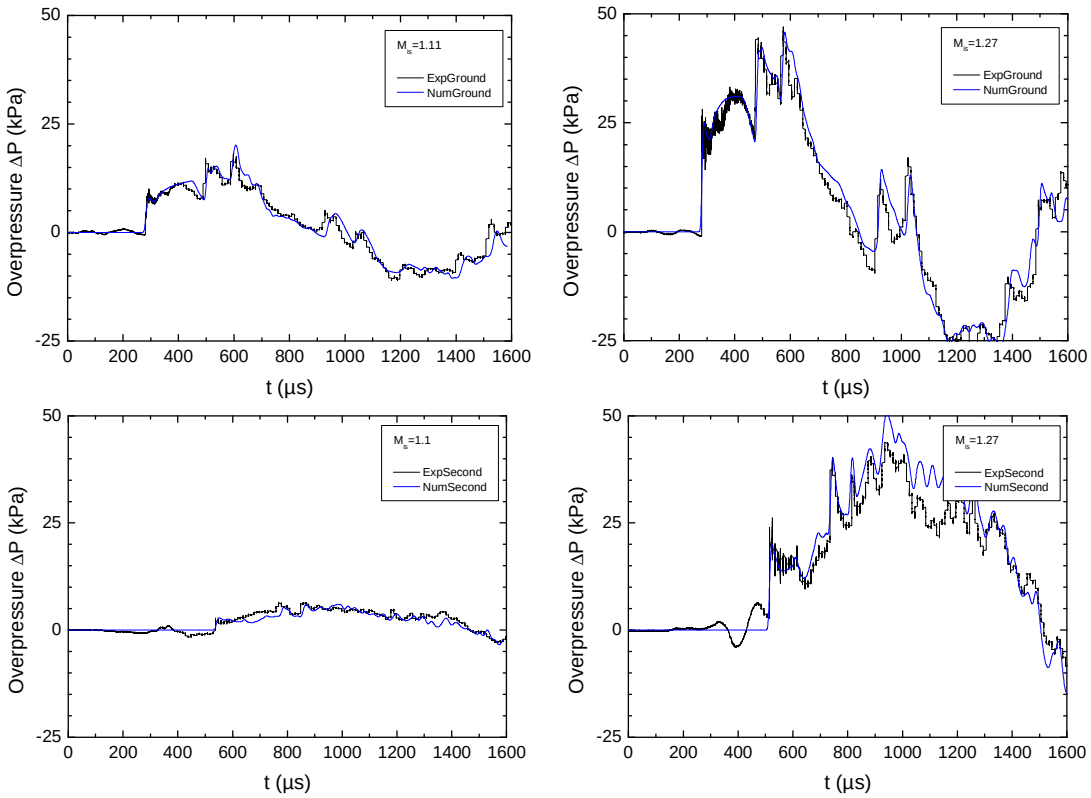

Figure 7: Comparison between experimentally and numerically obtained recorded pressures at the center of the first and the second floor's rear walls.

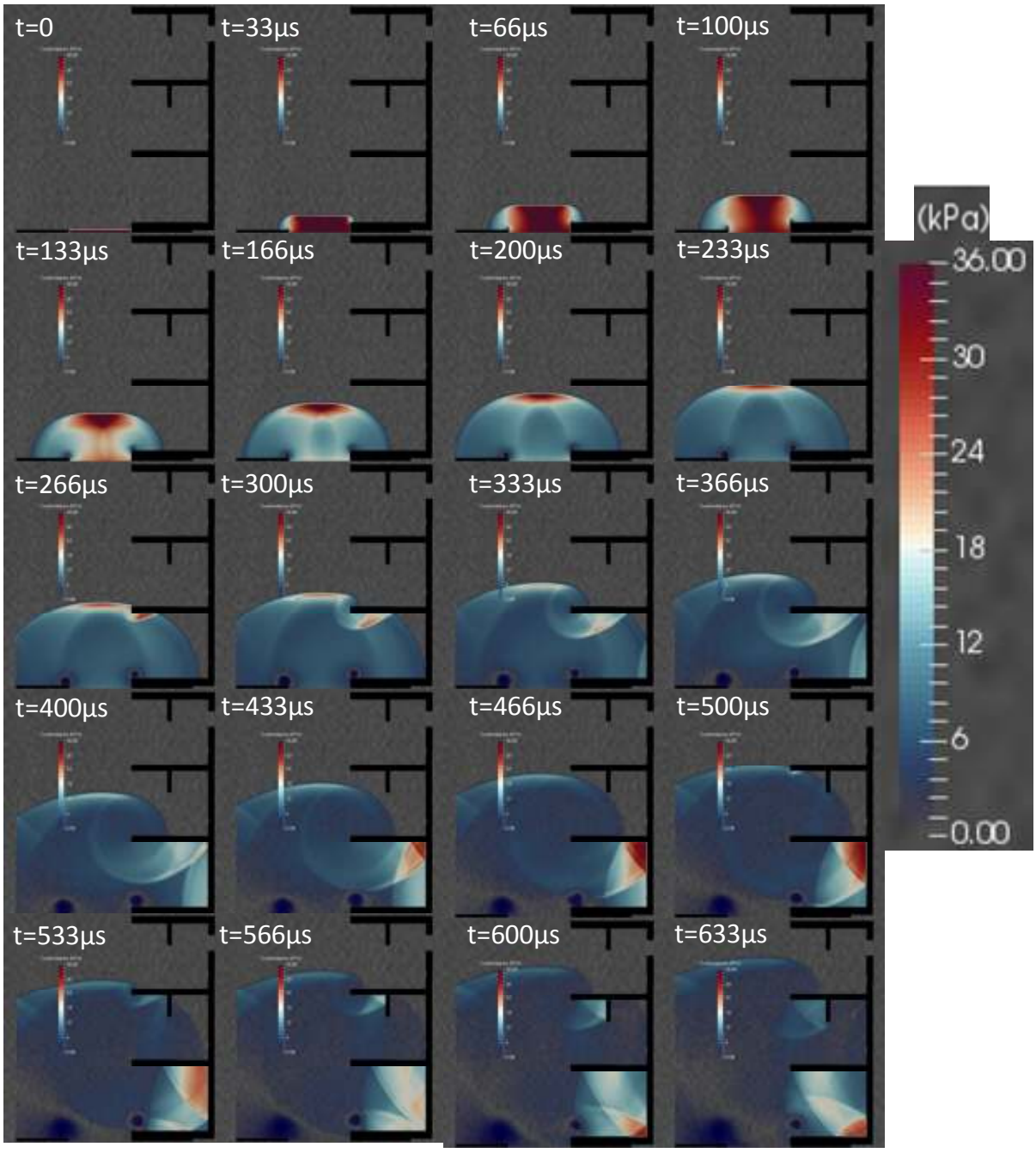

Figure 8: Numerical simulation (30,000 f/s) of pressure distribution inside the building model showing the evolution and multiple reflections of the entering blast wave. The incident shock wave Mach number inside the shock tube is 1.11 (T80#974).

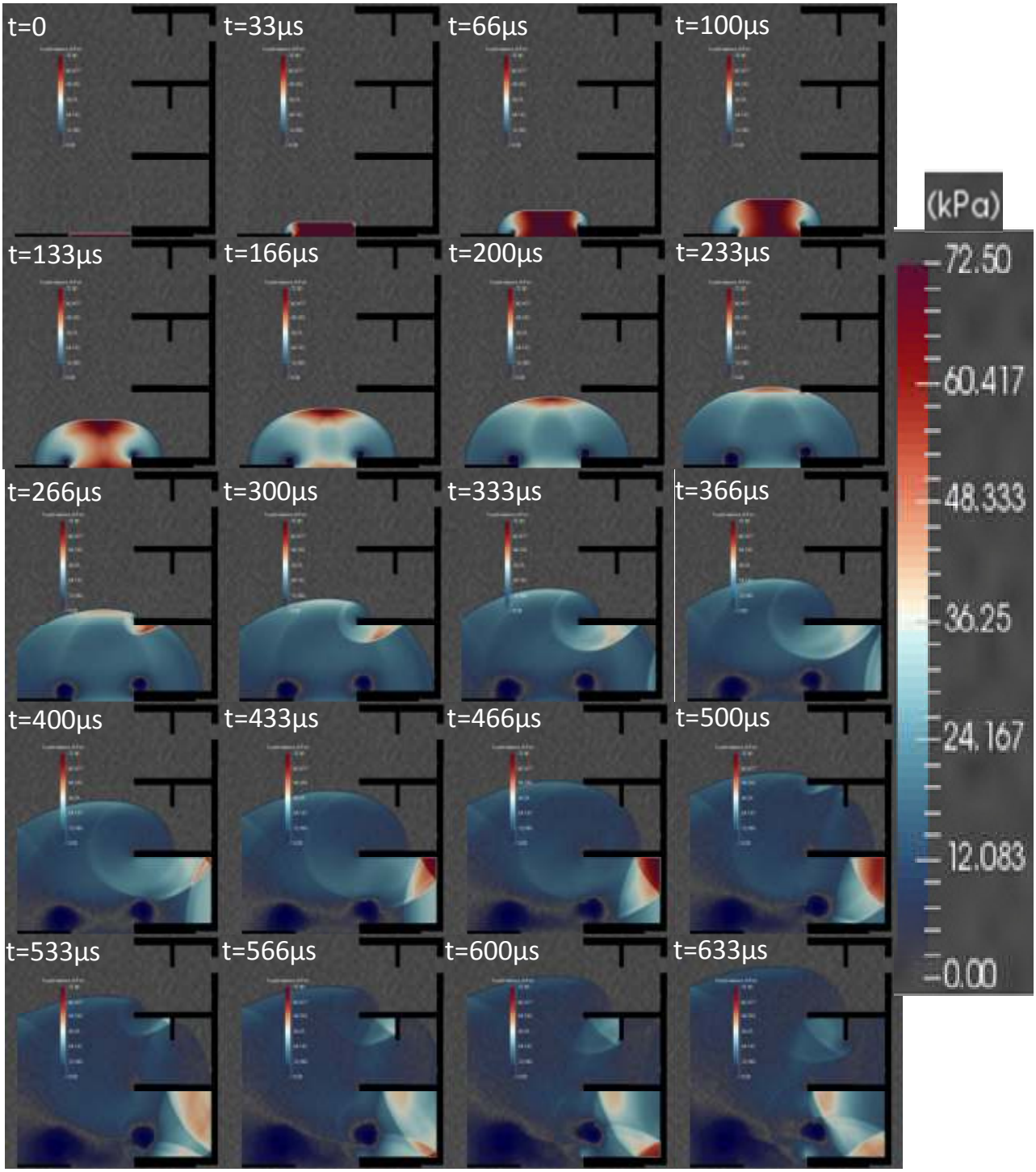

Figure 9: Numerical simulation (30,000 f/s) of pressure distribution inside the building model showing the evolution and multiple reflections of the entering blast wave. The incident shock wave Mach number inside the shock tube is 1.27 (T80#975).

the room ceiling and walls. The present work might be useful in designing building structures complying with safety standards, as well as for people who are not familiar with explosion generated blast waves.
Finally, the present work could also be helpful to validate numerical codes able to predict such effects without taking into account broken construction materials and glass debris, as well as primary blast effects in urban structures and complexes.

Acknowledgments:

The authors want to thank Justine Cintas, Safinah Mihidjay and Sofia Djouabri for helping in running the experiments within the field of the "Apprentis Chercheurs" Young Program in the framework of "l'Abre des Connaissances".

References :

[1] Debien B., Leclerc T., Clapson P., Perez J.-P., Lenoir B., Pats B. Lésions par explosion. MAPAR Conference (2006).
[2] Wright R. K. Death or injury caused by explosion. Clin Lab Med; 3:309-319 (1983).
[3] Technical Guide to the reference values of effects thresholds accidental phenomena of classified installations, French Republic, (October 2004).
[4] French Ministry of Ecology INERIS report realized after the disaster occurred on the NITROCHIMIE site on March the 27th 2003.
[5] Ben-Dor G., Shock Wave Reflection Phenomena. Springer (1992).
[6] Igra O., Falcovitz J., Reichenbach H., Heilig W., Experimental and numerical study of the interaction between a planar shock wave and a square cavity, J. Fluid. Mech. (1996).
[7] Ben-Dor G., Igra O., Elperin T. Handbook of Shock Waves, Academic Press, 2001.
[8] Jourdan, G., Houas, L., Schwaederlé, L., Layes, G., Carrey, R., and Diaz, F. "A new variable inclination shock tube for multiple investigations". *Shock waves*, 13(6), pp. 501–504, 2004.
[9] Toro, E. F., Riemann solvers and numerical methods for fluid dynamics: a practical introduction, Springer Science & Business Media (2009).
[10] van Leer, B. On the Relation Between the Upwind-Differencing Schemes of Godunov, Enguist-Osher and Roe. SIAM J. Sci. Stat. Comput., 5(1):1-20, 1985.
[11] Quirk J. J., An Alternative to Unstructured Grids for Computing Gas Dynamic Flows Around Arbitrarily Complex Two Dimensional Bodies. Computers and Fluids, 23(1):125-142, 1994.
[12] Van Leer, B., Towards the Ultimate Conservative Difference Scheme V. A Second Order Sequel to Godunov's Method. J. Comput. Phys., 32:lOl-136, 1979
[13] *Mpi: a Message-Passing Interface Standard*. Technical Report, University of Tennessee, Knoxville, TN, USA, 1994.
[14] E.F. Toro, M. Spruce and W. Speares, Restoration of contact surface in the HLL Riemann solver, Shock Waves, 4 (1994) 25-34